Heat transport in the high-pressure ice mantle of large icy moons

G. Choblet, G. Tobie, C. Sotin, K. Kalousová, O. Grasset

Heat transport in the high-pressure ice mantle of large icy moons

G. Choblet[a,*], G. Tobie[a], C. Sotin[b], K. Kalousová[b,c], O. Grasset[a]

[a] Laboratoire de Planétologie et Géodynamique, UMR-CNRS 6112, Université de Nantes, 2 rue de la Houssinière, F-44322 Nantes, France
[b] Jet Propulsion Laboratory, Caltech, 4800 Oak Grove Drive, Pasadena, CA 91109, USA
[c] Charles University, Faculty of Mathematics and Physics, Department of Geophysics, V Holešovičkách 2, 180 00 Praha 8, Czech Republic

ARTICLE INFO

Article history:
Received 30 May 2016
Revised 24 October 2016
Accepted 1 December 2016
Available online xxx

Keywords:
Ganymede
Titan
Callisto
Ices
Interiors

ABSTRACT

While the existence of a buried ocean sandwiched between surface ice and high-pressure (HP) polymorphs of ice emerges as the most plausible structure for the hundreds-of-kilometers thick hydrospheres within large icy moons of the Solar System (Ganymede, Callisto, Titan), little is known about the thermal structure of the deep HP ice mantle and its dynamics, possibly involving melt production and extraction. This has major implications for the thermal history of these objects as well as on the habitability of their ocean as the HP ice mantle is presumed to limit chemical transport from the rock component to the ocean. Here, we describe 3D spherical simulations of subsolidus thermal convection tailored to the specific structure of the HP ice mantle of large icy moons. Melt production is monitored and melt transport is simplified by assuming instantaneous extraction to the ocean above. The two controlling parameters for these models are the rheology of ice VI and the heat flux from the rock core. Reasonable end-members are considered for both parameters as disagreement remains on the former (especially the pressure effect on viscosity) and as the latter is expected to vary significantly during the moon's history. We show that the heat power produced by radioactive decay within the rock core is mainly transported through the HP ice mantle by melt extraction to the ocean, with most of the melt produced directly above the rock/water interface. While the average temperature in the bulk of the HP ice mantle is always relatively cool when compared to the value at the interface with the rock core ($\sim$ 5 K above the value at the surface of the HP ice mantle), maximum temperatures at all depths are close to the melting point, often leading to the interconnection of a melt path via hot convective plume conduits throughout the HP ice mantle. Overall, we predict long periods of time during these moons' history where water generated in contact with the rock core is transported to the above ocean.

1. Introduction

Ganymede, Callisto, and Titan, the largest icy moons in the Solar System, have similar mass and radius although their surface characteristics differ. Models of their interior structure are constrained by observations of the Galileo and Cassini missions (see Hussmann et al., 2015, for a synthesis). Moments of inertia (MoI) inferred from the gravity field suggest different degrees of differentiation for these three moons. Ganymede is fully differentiated into an iron core where the magnetic field is generated (Schubert et al., 1996; Kivelson et al., 2002), a rock mantle and a thick water layer including a high-pressure (HP) ice mantle, a liquid ocean and an outer ice I shell. Titan is less differentiated with a larger value of the MoI implying a larger and less dense core of hydrated silicates (Castillo-Rogez and Lunine, 2010), and Callisto is the least differentiated with possibly a mixture of ice and rock (McKinnon, 2006). In full agreement with space observations, interior structure models for these three moons favor the presence of a deep ocean between the icy crust and a layer of high pressure (HP) ice (Sohl et al., 2003; Sotin and Tobie, 2004; Vance et al., 2014).

Both the detection by the Huygens probe of an electric signal at 36 Hz with specific variations during the descent (Béghin et al., 2012) and Cassini's radio science measurement of a very large tidal Love number (Iess et al., 2012) are indeed best explained by the presence of a deep salted ocean. In the case of Ganymede and Callisto, the detection of an induced magnetic field by the Galileo spacecraft also suggests the presence of a subsurface electrically conducting ocean (Khurana et al., 1998; Kivelson et al., 2002) although measurements are not fully conclusive in the case of Ganymede. Subsequent modeling efforts confirm this hypothesis for Callisto (Lindkvist et al., 2015) and the detection of oscillating aurora ovals further points to the existence of a deep ocean within Ganymede (Saur et al., 2015).

* Corresponding author.
E-mail address: gael.choblet@univ-nantes.fr (G. Choblet).

between two ice layers results from a well-known feature of the water phase diagram (Bridgman, 1937) and has long been used to constrain thermal evolution models of Callisto and Ganymede (Kirk and Stevenson, 1987; Mueller and McKinnon, 1988; Showman et al., 1997) or Titan (Grasset et al., 2000; Tobie et al., 2005). However, all these models lack a specific description of heat transfer in the HP ice mantle. One of the aims of the present study is precisely to provide such a description.

Furthermore, the presence of the HP ice mantle prevents direct contact between the ocean and the rocky core. This contrasts with smaller moons with internal oceans such as Enceladus or Europa where such a contact is expected to occur during prolonged periods. While the latter is considered as a favorable property for being considered habitable (cf. e.g. Lammer et al., 2009), the existence of the HP ice mantle in large icy moons could inhibit the required chemical exchanges between the rock core and the internal ocean. The second goal of the present study is therefore to assess the degree of melt production and its impact on the heat and chemical transport through the HP ice mantle.

Evidence for at least a limited amount of chemical transfer between the rock component and the hydrosphere are provided by the Galileo and Cassini missions. The detection of ^{40}Ar, the decay product of ^{40}K initially contained in rocks, in Titan's atmosphere (Niemann et al., 2010), suggests that this chemical transfer lasted a sufficiently long period of time or occurred sufficiently late during the moon's evolution. In addition, gravity, shape and rotation measurements advocate for the presence of salts within the internal ocean to account for a relatively large density (Baland et al., 2014; Lefevre et al., 2014; Mitri et al., 2014). Similarly, the magnetic evidence for deep oceans within Ganymede and Callisto (Khurana et al., 1998; Kivelson et al., 2002; Saur et al., 2015) also implies minimum conductivity values that can be related to minimum salinity. However, it is unclear if these characteristics are inherited from leaching during aqueous differentiation processes or if they result from continuous exchange processes through the high-pressure mantle (Kargel et al., 2000). In order to assess the transport efficiency through the HP ice mantle, it is essential to better understand its dynamics and its possible thermal state.

Although laboratory experiments on the viscosity of high-pressure ices suggested very early that convection processes were likely (Poirier et al., 1981), the convective regime is still unknown. This is due to the difficulty to treat numerically the cold thermal boundary layer (TBL) at the ocean/ice interface where melting is predicted because the typical temperature profile in the cold TBL for subsolidus convection is steeper than the melting curve: conduction profiles already involve typical gradients of 0.5 K/km, larger than the temperature gradient along the melting curve at such depths (0.1–0.2 K/km). Thus, extraction of liquid water generated in the HP ice mantle is expected and may have a significant effect on the thermal budget.

Here, we describe 3D spherical simulations of subsolidus thermal convection tailored to the specific structure of the HP ice mantle of large icy moons. The conditions for melting to occur and the location of partial melt in the HP layer are investigated. Any melt produced within the HP ice mantle is treated in a simplified manner, assuming it is instantaneously extracted without taking into account the compaction of the matrix. Ice viscosity is temperature and pressure-dependent but does not include stress-dependency nor grain-size evolution. After describing the physical model we proceed with the main controlling parameters and the numerical treatment (Section 2), we present the results in Section 3, firs through a series of typical examples illuminating the effect of spe cific parameters, then through a global analysis. These are dis cussed in Section 4. Planetary implications are further developeu in Section 5.

We describe solid-state convection of the HP ice mantle in a fraction of a 3D spherical shell and numerical results presented below correspond to a statistical steady-state for heat transfer. While our purpose here is to derive a general scheme for large icy moons, dimensions and physical parameters are roughly tailored to the case of Ganymede. Although various polymorphs of high-pressure ice might appear if the HP ice mantle is thick enough (Hussmann et al., 2015), we focus here solely on ice VI and neglect phase transitions (in the following, unless stated otherwise, the term "ice" thus refers to ice VI as the single constituent of the HP ice mantle). Finally, we present the conservation equations in their dimensionless form, highlighting the role of dimensionless numbers, which will be useful for the description of a wider parameter range not entirely covered by our simulations. However, for the sake of clarity, we display model results with proper physical dimensions.

2.1. Physical model

The dynamics of the HP ice mantle is described by subsolidus thermal convection of the ice matrix with the instantaneous extraction of liquid water into the overlying ocean. A spherical geometry is considered between the rock-water interface located at $R_b = 1800$ km (cf. e.g. Husmann et al., 2015) and the HP ice mantle/ocean interface located at $R_s = R_b + d$ with d the thickness of the HP ice mantle, taking the values 100, 200, 350 km in the calculations presented here (see Table 2). Such values are chosen to mimic variations in global thickness throughout the moon's evolution that roughly reflect the variations in basal heat power from the rock core (larger heat fluxes are associated with thinner HP ice mantles). The corresponding values of the ratio f between the inner and outer radii are 0.85, 0.9, 0.94. Temperature at the HP ice mantle/ocean interface corresponds to the melting value at pressures corresponding to radius R_s (see Table 1): 307 K, 298 K, 281 K, associated respectively to $d = 100$ km (1110 MPa), $d = 200$ km (950 MPa), $d = 350$ km (710 MPa). The melting curve for ice VI in a pure water system is parameterized using the values proposed by Choukroun and Grasset (2007) and is also used to describe melting within the HP ice mantle.

Conservation of mass, momentum and energy are considered in the extended Boussinesq approximation. Their dimensionless form is

$$\nabla \cdot v = 0. \tag{1}$$

$$0 = -\nabla p^* + \nabla \cdot \tau - \mathrm{Ra}_f \theta e^r \tag{2}$$

$$\frac{\partial \theta}{\partial t} + v \cdot \nabla \theta = \nabla^2 \theta + \frac{\mathrm{Di}}{\mathrm{Ra}_f} \tau : \dot{\epsilon} + \mathrm{Di}(\theta + \theta_s) v^r \tag{3}$$

where v, p^* and θ are the velocity (radial component v^r), pressure and temperature fields, τ and $\dot{\epsilon}$ are the stress and strain-rate tensors and e^r is a unit vector in the radial direction. The following characteristic scales are introduced for length (d), time (d^2/κ, with κ the thermal diffusivity), temperature ($\Delta T = q_b d/k$, with q_b the basal heat flux and k thermal conductivity) and viscosity (η_s, i.e. the value at the surface of the HP mantle) - the symbols associated to all model parameters and their values are summarized in Table 1. The two resulting dimensionless numbers are the Rayleigh number

$$= \frac{\alpha \rho g q_b d^4}{k \kappa \eta_s} \tag{4}$$

the dissipation number

$$\mathrm{Di} = \frac{\alpha g d}{c_p} \tag{5}$$

Please cite this article as: G. Choblet et al., Heat transport in the high-pressure ice mantle of large icy moons, Icarus (2016), http://dx.doi.org/10.1016/j.icarus.2016.12.002

R_b =1800 km and thus depends on the value chosen for d. Similarly, the values for $f = (R_b + d)/R_b$ directly reflect the choice for d. *: the term 'surface' refers here to the surface of the HP ice mantle. The following references have been used for parameter values: [1]Bezacier et al. (2014), [2]Tchijov (2004), [3]Andersson and Inaba (2014), [4]Choukroun and Grasset (2007). The reference value for κ is $k/(\rho C_p)$. The latent heat L is determined from the slope of the melting curve.

Parameter	Symbol	Value/range	Unit
Thermal expansivity[1]	α	1.5×10^{-4}	K^{-1}
Heat capacity[2]	c_p	2700	J kg^{-1} K^{-1}
Gravity	g	1.6	m s^{-2}
Surface* viscosity	η_s	1.3×10^{16} - 1.3×10^{17}	Pa s
HP ice mantle thickness	d	$\in$ {**350, 200, 100**}	km
Thermal conductivity[3]	k	1.6	$Wm^{-1}K^{-1}$
Thermal diffusivity[1, 2, 3]	κ	4.3×10^{-7}	m^2 s^{-1}
Reference density[1]	ρ_s	1390	kg m^{-3}
Surface* (ice VI melting at R_s) temperature	T_s	$\in$ {**281, 298, 307**}	K
Latent heat[4]	L	360×10^3	J kg^{-1}
Dissipation number	Di	0.06 – 0.02	–
Ratio between inner and outer radii	f	$\in$ {**0.85, 0.9, 0.94**}	–
Rayleigh number	Ra_f	1.8×10^7 – 2.2×10^9	–

Table 2
List of calculations. P_b denotes the heat power out of silicate core and q_b the corresponding (basal) heat flux. d is the thickness of the mantle. η_s is the viscosity value at the interface between the ocean and the HP ice mantle. Ra_f is the flux based Rayleigh number computed with viscosity value η_s (see Eq. 4). For each of the 12 cases indicated here, four calculations have been performed: one without melt extraction and the "Durham rheology" (noted $\bullet_D$), one without melt extraction and the "homologous temperature rheology" (noted $\bullet_H$), one with melt extraction and the "Durham rheology" (noted $\bullet_D^m$), one with melt extraction and the "homologous temperature rheology" (noted $\bullet_H^m$).

Case #	P_b (TW)	q_b (mW.m^{-2})	d (km)	η_s (Pa s)	Ra_f
1	0.204	5	350	1.3×10^{17}	2.7×10^8
2	0.407	10	350	1.3×10^{17}	5.5×10^8
3	0.814	20	350	1.3×10^{17}	1.1×10^9
4	1.63	40	350	1.3×10^{17}	2.2×10^9
5	0.204	5	200	6.7×10^{16}	5.8×10^7
6	0.407	10	200	6.7×10^{16}	1.2×10^8
7	0.814	20	200	6.7×10^{16}	2.3×10^8
8	1.63	40	200	6.7×10^{16}	4.7×10^8
9	0.204	5	100	1.3×10^{16}	1.8×10^7
10	0.407	10	100	1.3×10^{16}	3.7×10^7
11	0.814	20	100	1.3×10^{16}	7.3×10^7
12	1.63	40	100	1.3×10^{16}	1.5×10^8

$\theta_s = T_s/\Delta T$ is the dimensionless temperature at the surface of the HP mantle (with T_s value in K). These conservation equations are complemented by the temperature and pressure dependence of viscosity, i.e. one of the two main parameters controlling the dynamics of the HP ice mantle (cf. 2.2).

A uniform temperature ($\theta = 0$) is prescribed at the surface, corresponding to the HP ice mantle/ocean interface. This interface is a free-slip boundary. A uniform heat flux q_b is prescribed at the bottom boundary, corresponding to the rock/HP ice mantle interface. This interface is a no-slip boundary although the possible presence of large amounts of liquid at this interface could motivate the use of a free-slip condition. The heat flux q_b is the second major controlling parameter varied among numerical experiments (cf. 2.3). The steady-state equilibrium is considered to be reached when the heat power supplied at the base of the HP ice mantle, $P_b = 4\pi R_b^2 q_b$, is equal within less than a few percents to the time average of the power extracted at the surface of the HP mantle both by thermal conduction, $P_{cond} = 4\pi R_s^2 k(\partial T/\partial r)_{r=R_s}$, and by transport of melt produced in the HP ice mantle, $P_m = L(dm/dt)$ (L is latent heat of fusion and dm/dt is the melting rate in kg s^{-1}),

$$P_b = P_{cond} + P_m \tag{6}$$

Melting and its effect on the transport of heat and mass is the main focus of the present numerical investigation with some calculations performed as reference cases without considering melting and others where it is introduced. As indicated above, we use a simple model to describe melt transport: if, subsequent to an advection time step of duration δt, temperature $\tilde{T}$ locally exceeds the melting temperature at a given location, the temperature is set back to the melting value $T_m(r)$ and the excess heat is used to produce liquid water at a rate inversely proportional to the latent heat:

$$\dot{x}_m = \frac{c_p}{L}\left(\tilde{T} - T_m\right)\delta t^{-1} \tag{7}$$

which assumes that latent heat produced locally associated to the melting rate $\dot{x}_m$ balances exactly this excess heat that is lost. In this model, water is supposed to be instantaneously extracted to the ocean and compaction of the matrix is neglected. These assumptions are discussed in Section 4.

2.2. Rheology of ice VI

Laboratory experiments have been performed to study the strength of ice VI (Poirier et al., 1981; Sotin et al., 1985; Durham et al., 1996). Values for the strain-rates in the high stress regime of these laboratory experiments agree reasonably well although the stress-dependence exponent differs significantly among the various groups of experiments (Fig. 1): Durham et al. (1996) report a large value of 4.5, typical of the stress-dependent creep of ice I observed at high stresses while Sotin et al. (1985) indicate a lower value of 1.9 from experiments conducted at temperature closer to the melting point. It is possible that at low strain-rates associated to the HP ice mantle dynamics (typically $< 10^{-11}$ s^{-1} in our numerical experiments), grain-size sensitive mechanisms contribute significantly to deformation. While these were not observed in the laboratory, they are documented for ice I and observed in glaciers (cf. Fig. 1). These would lead to a lower value of the stress exponent and Durham et al. (1996) report that such a transition might be present in the few experiments performed for ice VI at warmer temperatures relevant for our study ($T > 250$ K). Here, we assume a newtonian rheology mimicking this low-stress regime. Nevertheless, given the uncertainty associated with the extrapolation of experimental values to low-stresses (and the possibility of different

Please cite this article as: G. Choblet et al., Heat transport in the high-pressure ice mantle of large icy moons, Icarus (2016), http://dx.doi.org/10.1016/j.icarus.2016.12.002

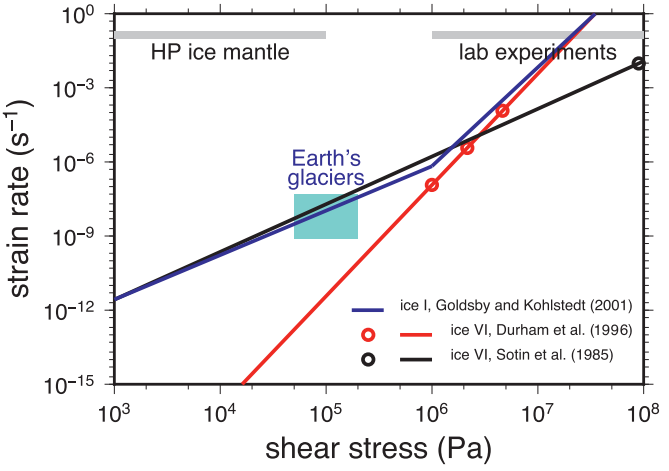

Fig. 1. Rheology of ice VI and ice I. Strain rate as a function of stress from experiments and glacier observations for ices close to the melting point. Circles refer to the laboratory measurements on ice VI (black: Sotin et al. (1985), red: Durham et al. (1996)). The black and red solid lines correspond to extrapolation of these values. The blue line indicates ice I rheology (Goldsby and Kohlstedt, 2001) with a change of regime from dislocation creep (high stress) to grain boundary sliding creep (low stress). The cyan rectangle shows the range observed in terrestrial glaciers (Hudleston, 2015) while the grey rectangles indicate the stress range in laboratory experiments for ice VI and the expected range in natural conditions for the HP ice mantle. (For interpretation of the references to colour in this figure legend, the reader is referred to the web version of this article.)

creep regime), a reasonable range covering the viscosity of ice VI in the HP mantle could be [10^{14}, 10^{18}] Pa s.

Viscosity follows a classical relationship:

$$\eta = \eta_s \exp\left[E^*\left(\frac{1}{RT} - \frac{1}{RT_s}\right) + V^*\left(\frac{p}{RT} - \frac{p_s}{RT_s}\right)\right] \quad (8)$$

with R the gas constant and p_s the pressure at the ocean/ice interface. The value for the activation energy E^* corresponds to the lower bound reported by Durham et al. (1996): 90 kJ.mol^{-1}. The activation volume V^*, measuring the influence of pressure, is not constrained by experiments. We thus use two end-member approaches: one using the estimate proposed by Durham et al. (1996) from measurements at lower temperatures ($T < 250$ K) and lower strain rates, $V^* = 10$ cm^{3}mol^{-1}. The second approach corresponds to the homologous temperature formulation: it assumes that viscosity remains constant with depth for a temperature profile corresponding to a given fraction of the melting temperature T_m, i.e. a relationship of the form:

$$\eta = \eta_s \exp\left[\gamma\left(\frac{T_m}{T} - 1\right)\right] \quad (9)$$

Compared to the Arrhenius relationship (Eq. 8), this is equivalent to prescribing an activation volume that varies with depth and whose value is globally larger than the one proposed by Durham et al. (1996). In order to compare the two formulations, we use the same temperature dependence at the surface of the HP mantle ($\gamma = (E^* + p_s V^*)/(RT_s)$).

The range of viscosity values investigated here ($\eta_s \in [1.3 \times 10^{16}, 1.3 \times 10^{17}]$ Pa s, see Table 2) is chosen independently of the HP ice mantle thickness (i.e. it is not computed from the (p,T) conditions at the ocean/ice interface). This globally involves average viscosity values in the bulk of the HP ice mantle that are one order of magnitude larger than the surface value which corresponds to the upper end of estimates extrapolated from the experimental measurements cited above. The consequences of our choice of relatively large viscosity values (guided by numerical limitations) are discussed in Section 4.

Note that we do not include the effect of the presence of melt on viscosity. This is in agreement with our assumption that any melt produced is extracted instantaneously (see Section 2.1). In the case of a less efficient melt transport, the presence of interstitial melt may reduce the viscosity, as observed experimentally on low-pressure ices (De La Chapelle et al., 1999). However, such an effect on HP ices is still unconstrained.

2.3. Heat flux from the rock core

In order to constrain a plausible range for heat flux out of the silicate core P_b, we refer to the thermal evolution models proposed by Tobie et al. (2006) for Titan considering the possibility of subsolidus convection in the rocky core (earlier models assumed an equilibrium between the heat flux out of the core and heat production within it by radioactive decay). Such models include successively after an initial differentiation: 1) a conductive cooling stage, 2) a transient convective cooling stage after the birth of the first convective instabilities, 3) a quasi-static convective cooling stage (see Choblet and Sotin, 2001, for more details). Tobie et al. (2006) considered three values for the radiogenic content (also possibly reflecting the hydration state of silicates), but differences are only modest in the outcome. Tidal heating in the rock core is neglected. In this model, the maximum heat power out of the silicate core probably coincides with the end of the transient cooling stage and might reach values up to 1.65 TW. Conversely, the epoch associated with the smallest heat flux is present-day with a minimum value of $\sim$ 0.5 TW. Table 2 summarizes the various families of numerical experiments considered. Heat fluxes q_b: 5, 10, 20 and 40 mW.m^{-2} correspond to global heat power P_b of 0.204, 0.407, 0.814, 1.63 TW, respectively. The first value is not realistic but it is introduced as a test case that results in the smallest amounts of melt. The three other values describe the possible range reached during the satellite evolution.

2.4. Numerical method

We use the finite difference numerical tool OEDIPUS (Choblet, 2005; Choblet et al., 2007) with a multigrid flow-solver and an explicit scheme for the conservation of energy. Advection terms are treated with a flux-limiter (Superbee) high-resolution method. Only one of the six blocks of the cube sphere grid mesh is considered. It includes 128 uniformly spaced cells in the r direction (corresponding to a grid spacing in the range 0.8-2.7 km depending on the global thickness considered for the HP ice mantle) and 64 in the two lateral directions (corresponding to a grid spacing of 44 km at the bottom of the shell). 12 cases have been considered (see Table 2), each corresponding to a combination among 4 heat flux values and 3 HP mantle ice thickness values. For each case, four calculations have been performed: one without melt extraction and the "Durham rheology" (noted $\bullet_D$), one without melt extraction and the "homologous temperature rheology" (noted $\bullet_H$), one with melt extraction and the "Durham rheology" (noted $\bullet_D^m$), one with melt extraction and the "homologous temperature rheology" (noted $\bullet_H^m$).

As described in Eq. 7, melt production only results in the practical condition that the temperature never exceeds the melting curve at any depth. The compaction of the ice matrix due to melt extraction is neglected so that the precise monitoring of the amount of melt is not required. Note that this approach differs from the one implemented by Moore and Webb (2013) to describe magma ascent as the dominant heat transfer mechanism at the surface of the Archean Earth, for example, where cold lithosphere is added and advected downwards to conserve mass in the heat-pipe framework. Here, instead, we assume that the mass loss caused by melt extraction is always balanced by the cooling of the internal ocean

Please cite this article as: G. Choblet et al., Heat transport in the high-pressure ice mantle of large icy moons, Icarus (2016), http://dx.doi.org/10.1016/j.icarus.2016.12.002

so that, in effect, the thickness of the high-pressure mantle remains constant. The validity of this assumption is discussed in Section 4. Overall, the effect of melting enters mass conservation only at the global scale via the use of this assumption. The effect of melting on the conservation of energy is however considered locally through the local decrease of temperature (Eq. 7) and globally as the power extracted by melt enters the heat balance (Eq. 6).

3. Results

3.1. Selected set of simulations

Fig. 2 reports five examples of radial profiles corresponding to various bottom heat flux and rheological laws. Case 1_D is a reference calculation for which melting is ignored, leading to unrealistic temperatures larger than the melting point in the upper part of the layer. The temperature profiles (maximum, horizontally averaged and minimum temperatures, Fig. 2-a, left) thus result only from the geometry of the HP ice mantle and the rheology. While the extended Boussinesq approximation is considered, the effect of viscous dissipation and adiabatic heating/cooling on the radial gradient in the convective core is negligible. Although the reduction in viscosity caused by the temperature increase and the increase caused by the pressure effect are only moderate (Fig. 2-a, center), the thermal structure departs already significantly from isoviscous scaling relationships: for this geometry, the expected ratio between the temperature drops across the hot and cold boundary layers is 1.27 for an isoviscous fluid in the Boussinesq approximation (Choblet, 2012) while its value here is ~ 2.2. Note that this difference could in principle be attributed to the fact that the basal boundary condition is no-slip while the surface boundary condition is free-slip; however, Cartesian numerical experiments report a smaller effect of about 10% (Choblet and Parmentier, 2009). This case underlies the need to account for melting since temperatures exceed the melting point in the cold boundary layer and in the region below it, even in the case of an extremely low, probably unrealistic, basal heat flux.

The introduction of melting (2_D^m, also corresponding to a twice larger heat flux compared to case 1_D, Fig. 2-b) first causes the maximum temperature at a given depth to remain smaller or equal to the melting temperature. The maximum temperature is equal to the melting value in the upper 120 km of the mantle ($\sim 1/3$ of the HP ice mantle thickness). These profiles correspond to time-averages. In the 20–30 km-thick uppermost region where the horizontal average is close to the melting curve, melting occurs at all times at that depth, although not everywhere: while a little contribution to horizontal average, zones associated to the minimal temperature are always colder than the melting point. It is also worth noting that melt is produced in small amounts within a region where the average maximum temperature is below the melting temperature (between radii 1910 and 2030 km, Fig. 2-b, green curve in the right panel): this corresponds to intermittent melt production in this depth range. Below lies a region where melt is never produced and where the maximum temperature is always smaller than the melting point. In practice, this melt-free layer (of thickness $d_{\mathrm{NML}} \simeq 100$ km) is associated to zero permeability. We term it "no-melting layer" in the following. Our assumption of instantaneous upward melt extraction by porous flow does not hold in this region, which is discussed in Section 4. The average temperature eventually approaches the melting value to less than 1 K in the upper 30 km. As a consequence, the amount of heat conducted through the cold boundary layer is dictated by the slope of the melting curve at the ocean/ice interface. This value is almost identical for all calculations that include melting and does not depend on the HP ice mantle thickness. Due to a more efficient heat transfer associated to melt extraction, the introduction of melting also reduces the average temperature in the bulk of the layer (from ~ 7 K, Fig. 2-a, to ~ 5 K, Fig. 2-b although the basal heat flux is twice larger in the latter case). The viscosity is slightly increased accordingly. The maximum downwelling velocity is also reduced as well as the maximum upwelling velocity (Fig. 2-b, center right). Concerning upwelling velocity, melt extraction in the upper region also inhibits the warm ice plumes ascent as their relative buoyancy gets negligible. The melting rate at the base of the HP ice mantle is comparable to rates observed in the upper region. This basal melting region is extremely thin (restricted to the first grid layer immediately above the interface in our models). It is likely that a refined resolution might modify the melting rates obtained there. However, the temperature at the base of the HP ice mantle is dictated by the inward flux from the rock core and the global energy balance ensures that the order of magnitude of the melting rate in this region is correct: even in cases with larger heat fluxes (Fig. 2-d and e), resulting in significantly larger basal melting rates, its contribution to global melting is negligible. Note also that for the maximal values of the basal heat flux investigated here, that probably correspond to an early stage of the moon's evolution, the melting rate could induce an efficient thinning of the HP ice mantle typically corresponding to 1–3 km/Myr.

Compared to the case with the Durham rheology (2_D^m), the case with the homologous temperature formulation (2_H^m) leads to a significantly larger viscosity increase with depth (~ 300 instead of ~ 30, Fig. 2-b and c) due to an increasing distance between an almost uniform average temperature in the bulk of the layer and the melting point that increases with depth. This has a two-fold effect: 1) the heat extracted by warm ice instabilities from the bottom boundary layer is not as efficient but, 2) as these reach the melting value much deeper (50 km above the rock/ice interface, instead of 230 km), heat extraction is globally increased. As a consequence, the average temperature is $\sim 1-2$ K smaller than in the Durham case. Both the average upwelling and downwelling velocities are strongly reduced due to the larger viscosity in the lower half of the layer. Globally, cold plumes are strongly inhibited (viscosity is larger, buoyancy is smaller). The overall shape of the average temperature profile tends to be characterized by basal heating and internal cooling only (with heat sinks corresponding to melting), as the upper cold boundary layer vanishes, although not completely.

The case with a 40 mW.m^{-2} basal heat flux (case 4_D^m, Fig. 2-d), which corresponds to a 4-fold increase when compared to case 2_D^m (Fig. 2-b), does not result in a significantly different average temperature profile, except in the lowermost region as the average temperature now reaches the melting point at the rock/HP ice interface. As a consequence, the viscosity profile is similar to case 2_D^m and the downwelling velocity profile is comparable. The warm ice plumes are however much hotter than in case 2_D^m. Their temperature reaches the melting curve at all depths, except for a region located between 15 km and 150 km above the rock/ice interface. This increased relative buoyancy of warm plumes compared to case (2_D^m) also leads to strongly increased ascending velocities. In summary, the significantly larger basal heat flux is accommodated by hotter and faster hot instabilities eventually reaching the melting curve in the bulk of the layer. The thermal structure of colder ice remains practically unchanged. These conclusions remain valid for case 4_H^m (Fig. 2-e) when compared to lower heat flux case 2_H^m. In this case, the maximum temperature profile reaches the melting temperature (within 1 K) at all depths.

Fig. 3 provides further insights into the temperature field corresponding to case 4_D^m. The vertical cross section in Fig. 3-a illustrates how hot plumes are dominant and how colder downwellings are broad (and passive, see blue velocity in Fig. 2-d). As the temperature cannot exceed the melting point at a given radius, the hot plumes progressively cool as they ascend. Non-Boussinesq

Please cite this article as: G. Choblet et al., Heat transport in the high-pressure ice mantle of large icy moons, Icarus (2016), http://dx.doi.org/10.1016/j.icarus.2016.12.002

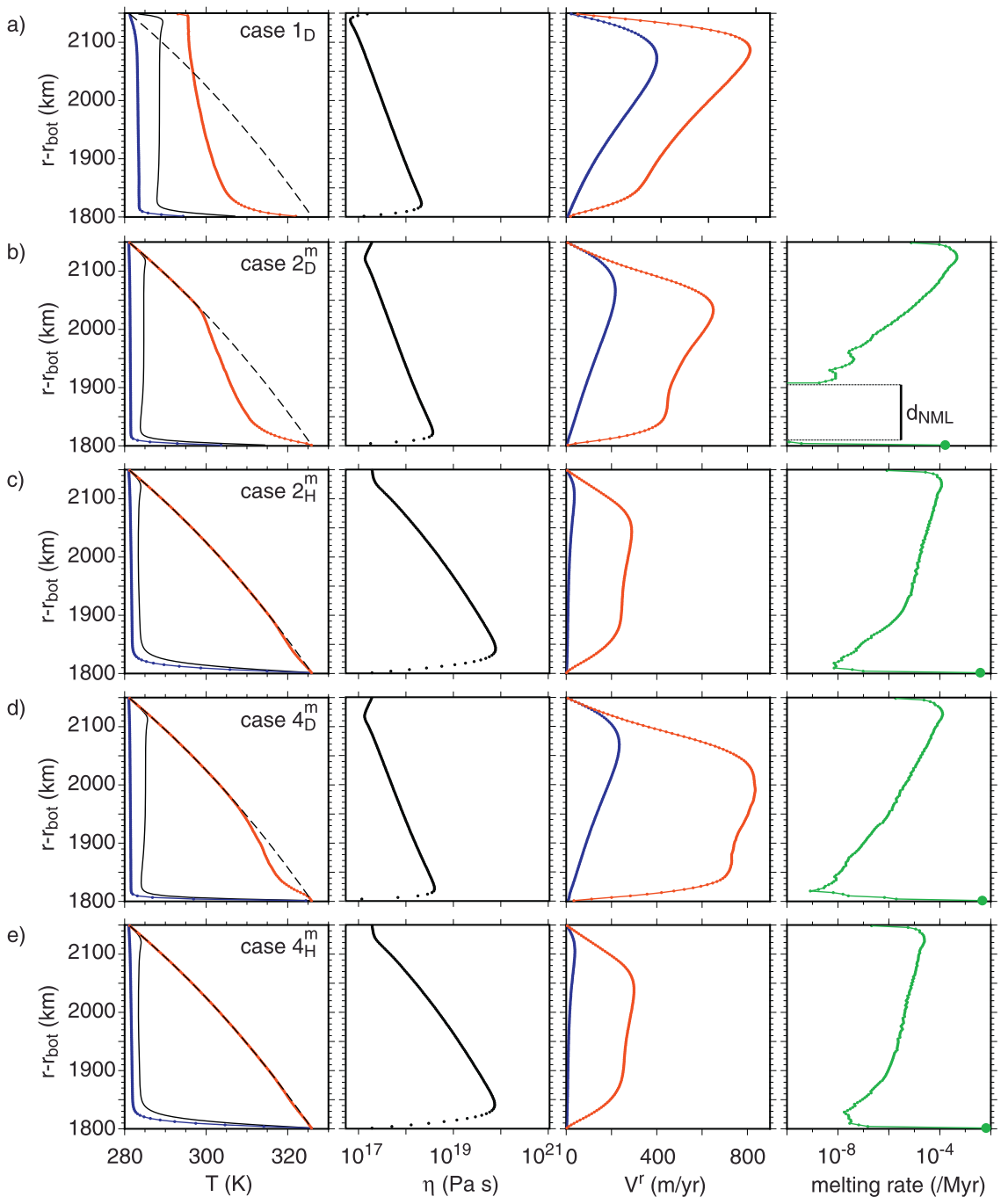

Fig. 2. Radial profiles for five selected numerical experiments: a) 1_D, b) 2^m_D, c) 2^m_H, d) 4^m_D, e) 4^m_H. *left* - minimum (blue), lateral average (black) and maximum (red) temperature as well as the melting temperature (dashed) at a given radius. *center left* - average viscosity at a given radius. *center right* - maximum upwelling (red) and downwelling (blue) velocity. *right* - lateral average of the melting rate at a given radius (expressed as the fraction of ice that melts per Myr at a given radius). A green half-disk at the bottom of each curve specifically indicates the melt produced immediately above the rock/HP ice interface. In panel b), d_{NML} denotes the thickness of the "no-melting layer", i.e. the region where no melt is produced and where the maximum temperature is at least 1 K colder than the melting point (see text). (For interpretation of the references to colour in this figure legend, the reader is referred to the web version of this article.)

compressibility effects (adiabatic cooling due to rising plumes or viscous heating in regions of large dissipation) are not distinguishable in this cross-section. In the uppermost region where the whole temperature field is close to the melting point, the plumes are not distinguishable and their buoyancy vanishes. Figure 3-b, corresponding to the same cross section, displays the temperature difference from the radially-dependent melting curve. Two regions are subjected to melting anytime and everywhere at a given radius: these are located immediately above the rock/ice interface and beneath the ice/ocean interface, the latter corresponding in practice to a much reduced melt production (Fig. 2-d). Between these two regions, melt occurs only in regions hotter than average corresponding to ascending plumes while the bulk of the mantle is cool. Fig. 3 also shows that the most developed hot plumes correspond to conduits of regions at (or close to) the melting point, interconnected from top to bottom. These conduits have a minimal radius at a depth of a few tens of kilometers above the basal interface.

Please cite this article as: G. Choblet et al., Heat transport in the high-pressure ice mantle of large icy moons, Icarus (2016), http://dx.doi.org/10.1016/j.icarus.2016.12.002

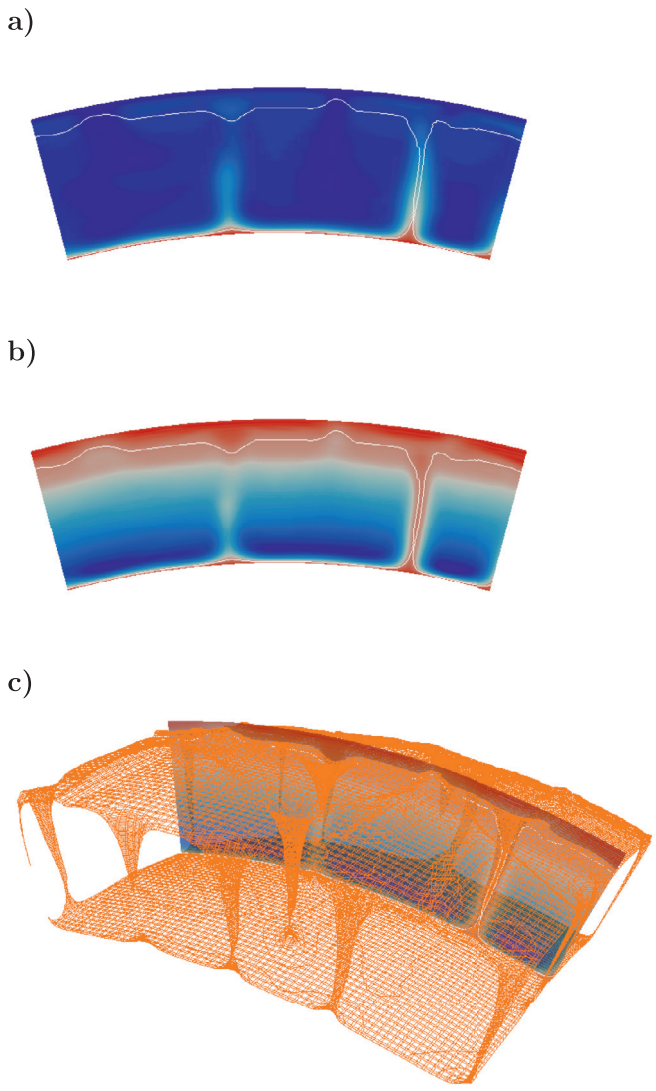

Fig. 3. Snapshot of the temperature field for case 4_D^m. a) vertical cross section for the temperature field T. The color scale ranges from 281 K (blue) to 326 K (red). b) same cross section for the difference between the temperature and the melting temperature at a given depth $T - T_m$. The color scale ranges from -43 K (blue) to 0 (red). c) perspective representation of the isotherm (orange) corresponding to a temperature value 1 K below T_m also reported on a) and b) as a white line. (For interpretation of the references to colour in this figure legend, the reader is referred to the web version of this article.)

3.2. Synthesis

Fig. 4 displays global results that allow the appraisal of all numerical experiments. First, as expected, the fraction of the heat power transported by melt extraction P_m/P_b (Fig. 4-a) increases as the basal heat flux is increased. As all models involve melting below the ocean/ice interface, the surface conductive heat flux is dictated solely by the slope of the melting curve there so that increasing the basal heat flux P_b is necessarily accommodated by a larger fraction of heat extracted by melt P_m. This fraction does not depend on rheology. The dependence on HP ice mantle thickness d reflects the slope of the melting curve at the ocean/ice interface, steeper at larger pressures, i.e. deeper locations of the interface. For reasonable values of the basal heat flux for large icy moons such as these reported by Tobie et al. (2006), the overall result is that conduction through the cold boundary layer in the HP ice mantle contributes only marginally to the heat transfer to the ocean: probably less than 10%, whatever the ice rheology and mantle thickness are.

The average temperature in the HP ice mantle is only a few K larger than the value prescribed at its surface (Fig. 4-b) as the temperature field is dominated by large and slow cold downwelling with only a few narrow hot plumes. It mostly depends on the mantle thickness controlling the convective vigor. Note that increasing the basal heat flux does not significantly affect this bulk temperature difference. While the average temperature characteristic of the bulk (almost isothermal) mantle was found to decrease in the case of the homologous temperature rheology (Fig. 2-b,d and c,e), the hot boundary layer is also warmer. The volumetric average over the whole mantle $< T >$ is therefore fairly independent of rheology.

Fig. 4-c displays the amount of melt production occurring at the ice/rock interface (more precisely, in the discrete layer immediately above) relative to the global melt production in the HP ice mantle. In all cases, this fraction increases with increasing basal heat flux: as soon as the basal heat power exceeds 500 GW, more than 50% of the melt is produced at the base of the layer except for the thickest mantle in the case of the Durham rheology (red circles). Overall, Fig. 4-a,c thus indicate that most of the heat originating in the rock core is used to melt the ice at the ice/rock core interface. In the present model, any parcel of water is simply removed from the HP layer and placed into the overlying ocean.

Fig. 4-d compiles the average thickness d_{NML} of the "no-melting layer" in the HP ice mantle. Only 5 cases out of the 24 models, display such a zero permeability layer. For these specific cases corresponding to (unrealistically) low values of the basal heat flux (P_b < 500 GW), the molten region in the bulk of the HP ice mantle is disconnected from the partially molten ice/rock interface. In the majority of cases however, as shown in the example of case 4_D^m (Figs. 2-e and 3), melt conduits in hot plumes actually provide an interconnected path for melt extraction. Furthermore, an additional numerical experiment (not shown here) indicates that this interconnected melt path is observed even for much thicker HP ice mantles: a case corresponding to the parameters of case 2_H^m but with a 550 km-thick HP ice mantle (from R_b =1600 km to R_s =2150 km) presents comparable or larger melting rates at all depths. Implications are discussed below (Section 4).

4. Discussion

For numerical reasons, this paper considers rather large values for the viscosity of ice VI near the melting point η_s. Smaller values can be envisioned leading to larger Rayleigh numbers (thus requiring refined resolution for the grid mesh in the numerical models). Extrapolation from the present results (Rayleigh number in the range 1.8×10^7 – 2.2×10^9) is however possible since both the reference viscosity and the basal heat flux enter the definition of the Rayleigh number (Eq. 4): for a given HP ice mantle thickness, and thus a given melting curve, increasing the basal heat flux is strictly equivalent to decreasing the reference viscosity by the same factor. The consequences of considering lower viscosities values should thus be the following: larger fractions of heat will be extracted through melting (Fig. 4-a), corresponding essentially to melt produced immediately above the ice/rock interface (Fig. 4-c). The bulk temperature of the HP ice mantle should remain relatively cold in average (Fig. 4-b), but a possible "no-melting layer" will tend to vanish as the maximum temperature at a given depth will increase up to the melting point (Fig. 4-d). Overall, all the above conclusions will thus be enforced.

In our model, liquid water is instantaneously extracted. This assumption is clearly debatable if a cold region with no-melting (cf. Figs. 2-b and 4-d) is present above the location of melt production as this would prevent upward porous flow. In a few cases

Please cite this article as: G. Choblet et al., Heat transport in the high-pressure ice mantle of large icy moons, Icarus (2016), http://dx.doi.org/10.1016/j.icarus.2016.12.002

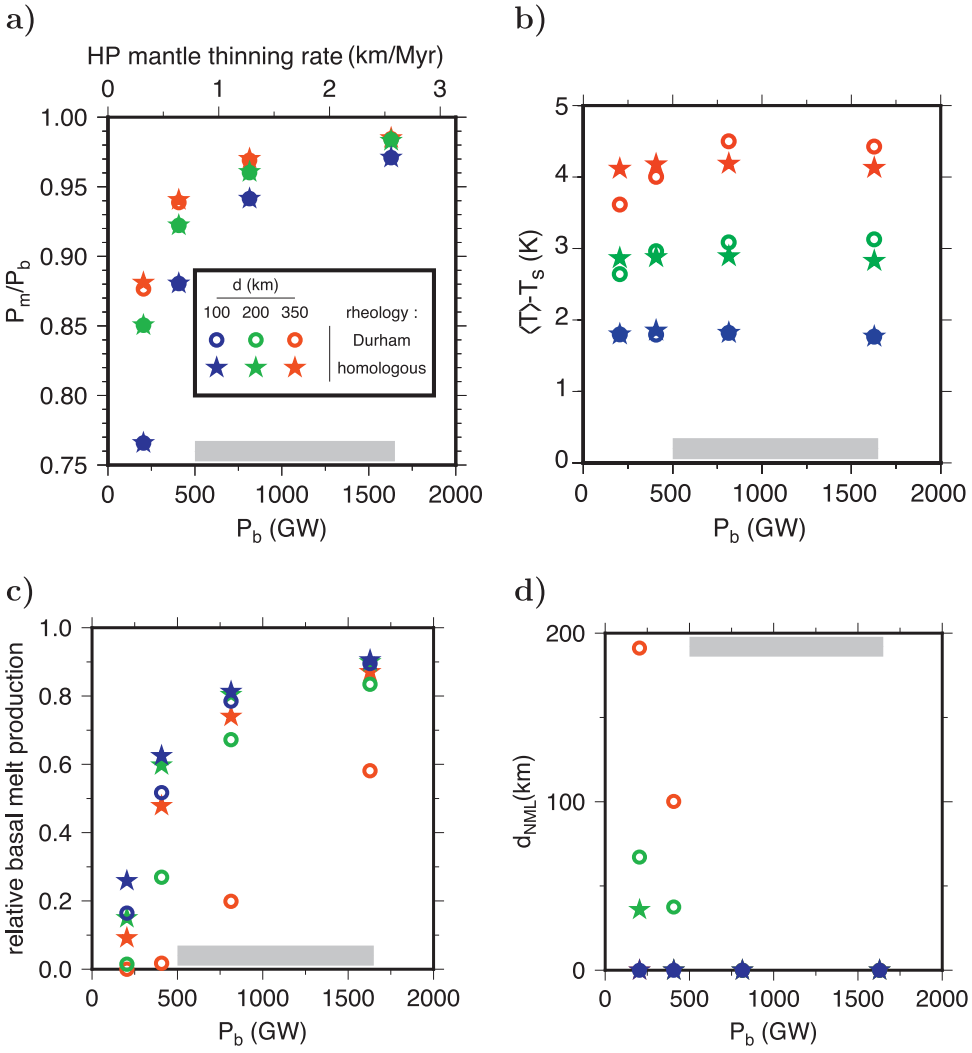

Fig. 4. Global results for all numerical experiments. Colors denote the value of the mantle thickness d: 350 km (red), 200 km (green), 100 km (blue). The shape of symbols denotes the rheology: homologous temperature formulation (stars), Durham estimate (circles). The grey rectangle indicates the possible range for basal heat flux reported for Titan by Tobie et al. (2006). a - Fraction of the heat that is transported by melt extraction at the surface of the HP mantle, cf. Eq. 6 (0: all heat conducted through boundary layer, 1: all heat extracted by melt - ideal case for an infinite value of P_b as P_{cond} has a non-zero finite value). The alternative x-axis indicates the production rate of liquid water (in km/Myr) if all the heat from the rock core were used to melt ice ($P_m/P_b = 1$) - a radius of 1800 km is used as a reference. b - Average temperature increase in the HP ice mantle $\langle T \rangle - T_s$, where $\langle T \rangle = \int_V T dV$. c - Fraction of the melt produced at the ice/rock interface. d - Thickness d_{NML} of the "no-melting layer" i.e. the layer where either melt production is null or where the maximum temperature is at least 1 K colder than the melting point. (For interpretation of the references to colour in this figure legend, the reader is referred to the web version of this article.)

corresponding to a small basal heat flux, a thick mantle and Durham rheology, such a configuration occurs at the base of the HP ice mantle. Furthermore, the ice matrix might remain impermeable even for regions where melting occurs. The ratio of the relative energies of solid/solid and liquid/solid interfaces (dihedral angle) controls the interconnectivity of a liquid network (Bargen and Waff, 1986). It is not measured for the ice VI/liquid water system so that permeability of HP ice is uncertain and might involve a 'percolation' threshold, i.e. permeability would remain effectively very small beneath a critical value of the porosity (shown by Golden et al., 1998, to possibly amount to as much as $\sim$ 5% in the case of terrestrial sea ice). In the eventuality of a significant value of the percolation threshold, only a fully biphasic formalism for solid ice and liquid water addresses the details of melt extraction (cf. e.g. Kalousová et al., 2014, although (at least) 2D models are required for this specific problem). We nevertheless argue that even in the case of impermeable ice, the positive bulk buoyancy of the solid matrix with internal pockets of liquid water will provide a mechanism to advect liquid pockets in the upper parts of the mantle (see Tobie et al., 2003, for a symmetrical case of a negative bulk buoyancy in the case of liquid pockets in ice Ih). In a study investigating this other end-member for melt extraction in the HP ice mantle of large icy moons, Kalousová et al. (2015) show that this mechanism will eventually lead to melt extraction on longer time scales than assumed here (although still modest, typically smaller than 10 Myr).

The influence of non water compounds is omitted in our models and a detailed description is beyond the scope of the present study. Their main effect on the system studied here would concern the melting curve and the density of the liquid phase (cf. e.g. Vance et al., 2014). Large concentrations of impurities in the ocean (either acquired during the differentiation or due to subsequent water-rock interactions) might deflect the melting curve. A significantly colder ocean, strongly enriched in ammonia (Choukroun and Grasset, 2010), or with a weaker effect, in magnesium sulfates (Vance et al., 2014), could lead to partial refreezing of the ascending hot conduits observed in our models, as these near the ocean/ice interface. Such a cold interface does not necessarily

Please cite this article as: G. Choblet et al., Heat transport in the high-pressure ice mantle of large icy moons, Icarus (2016), http://dx.doi.org/10.1016/j.icarus.2016.12.002

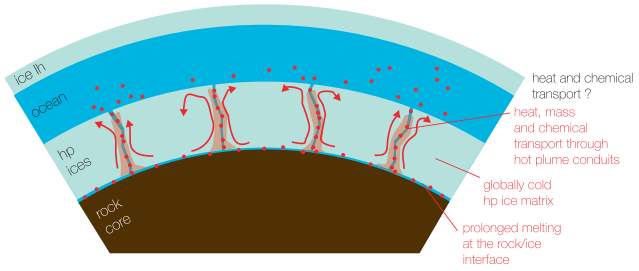

Fig. 5. Scheme for the principle of heat pipe transfer in the HP ice mantle.

prevent melt flow (cf. magma eruption at mid-ocean ridges on the Earth), especially for large amounts of melt but specific two-phase models are required to address the details of liquid water extraction to the ocean. Non water compounds could also be present at the base of the HP ice mantle as a result of rock alteration at the rock/ice interface. Nevertheless, if large amounts of melt produced there are extracted efficiently (as assumed here), concentrations will be small, especially if large pressures inhibit water-rock interactions (Vance et al., 2007). However, even present in small concentrations, contaminants may decrease the melting point by a few kelvins (Bollengier et al., 2013; Journaux et al., 2013; Vance et al., 2014), thus favoring the presence of melts in hot plumes, throughout the whole layer. The scheme presented above for the extraction of basal melting should not be altered significantly.

In our series of calculations, the thickness of the HP ice mantle and the basal heat power have been varied independently to investigate a large spectrum for the dynamics of the HP ice mantle: in reality, it is the balance between the heat that can be expelled at the surface through the ice I layer, and the heat that is introduced from the core, that fixes the dynamics and the thicknesses of the icy layers. In our models, we assume equilibrium between the extraction of melt produced in the mantle, causing the thinning of the HP ice mantle, and the cooling of the ocean, responsible for the thickening of the HP ice mantle. Maximum melting rates leading to the thinning of 2 km/Myr coinciding with the largest amounts of heat expelled from the rock core (e.g. when it starts convecting) would be balanced by cooling rates of 0.5 K/Myr for the ocean which remain reasonable. Ultimately, only a full description of heat transfer in the entire hydrosphere (HP ices/deep ocean/ice Ih) will allow to derive thermal history and test whether global melting rates derived above are stable (i.e. can be accommodated by surface heat flux). Such models shall be introduced with an updated description of the HP ice mantle along the lines described in the present study.

5. Planetary implications

Fig. 5 summarizes our findings and interpretations: the heat power produced by radioactive decay within the silicate core of large icy moons is mainly used to melt the ice. In our model where melt is instantaneously transported to the ocean, this extraction of melt is the main process to transfer heat coming out of the rocky core. The average temperature in the HP ice mantle is always cool when compared to the value at the interface with the rock core (only $\sim$ 5 K above the melting value at the interface with the ocean) and mostly depends on its global thickness. Maximum temperatures at all depths, nevertheless, are likely close to the melting point, often leading to the interconnection of a melt path. Finally, most of the melt is produced deep in the HP ice mantle (above the interface with the rock core) with only a marginal fraction in the bulk of the layer and in the cold boundary layer beneath the ocean.

The convection process responsible for efficient melt extraction towards the ocean in our models is equivalent to the heat-pipe mechanism initially introduced to explain the paradoxical observations of Io (O'Reilly and Davies, 1981): the Voyager spacecraft witnessed large reliefs suggesting the mechanical support of a strong (i.e. thick and cold) lithosphere, while the estimation of a huge surface heat flux from infrared spectroscopy favored a thin conducting lithosphere. Efficient heat transfer by fast melt extraction through a number of magmatic channels in an otherwise relatively cold and conductive lithosphere enables to solve this paradox. Similar mechanisms were also proposed for Venus (Turcotte, 1989) and mimicked through boundary conditions of convection models for subsequent studies of Io (Monnereau and Dubuffet, 2002) or the Archean Earth (Moore and Webb, 2013). In our study, the heat pipe mechanism occurs in a planetary layer whose upper interface corresponds to a phase change. Our results are immediately relevant for similar layers of HP ice polymorphs proposed to develop within water-rich exoplanets (Sotin et al., 2007; Grasset et al., 2009). While thick oceans have been considered to decrease the level of habitability of such objects (Noack et al., 2016), heat pipes in the high-pressure mantle constitute an efficient way to ensure chemical transfer from the interior to the ocean. Although a different context, as basal heating is not present, melting in the inner core of planets might also involve heat pipe and could be considered as one mechanism leading to the possible stratification observed at the base of the Earth's liquid core (Deguen, 2012).

Our result on a cold HP ice mantle rests on the assumption that melt is extracted instantaneously: while other conclusions hold in the other end member model for melt extraction, the bulk of the mantle could be warmer if the ice can retain a significant amount of interstitial melt (Kalousová et al., 2015). Low bulk temperature values in general imply that, on average, the viscosity of the HP ice mantle tends to be large. This should favor the detection of a large tidal resonance if a deep ocean is present within Ganymede (Kamata et al., 2015) with the measurement proposed by the Ganymede Laser Altimeter (GALA) as part of the JUICE mission (Grasset et al., 2013).

Overall, our models suggest that the transport of liquid water from the surface of the silicate core to the ocean is very likely, up to at least 500 Myr ago, i.e. when a large basal heat flux out of the core ($>$ 700 GW) prevailed. Such a transport might have ceased if the HP ice mantle is thicker than 300 km at present and if the rheology involves only a mild viscosity increase with pressure (Durham estimate rather than homologous temperature formulation). We thus predict that long periods during the history of large icy moons certainly involve chemical exchanges between the rock core and the ocean.

Finally, the above generic model seems to deliver a unique message for the three large icy moons considered in this study. It may thus lead to the incorrect notion that the fate of the HP ice mantle is identical for all three moons. As the observed surfaces of Titan, Ganymede and Callisto differ so obviously, a legitimate consequence would then be that the deep HP ice mantle is not responsible for this variety and thus that the deep interior does not influence the nature of the surface of these moons. At least two reasons exist however that could lead to different realizations of the same simple model for the three moons. First, the internal structure (hydrosphere structure and extent of the deep interior's differentiation) is expected to vary significantly among these objects. Moments of inertia inferred for the three moons vary between 0.31 (Ganymede) and 0.34-0.35 (Titan and Callisto) which suggests various degrees of differentiation (see Hussmann et al., 2015). This would naturally lead to a different geometry for the HP mantle (radius of the rock core/HP ice mantle interface). Second, various bulk compositions are to be expected for the three moons related to differences in the accretion process (both in time and

Please cite this article as: G. Choblet et al., Heat transport in the high-pressure ice mantle of large icy moons, Icarus (2016), http://dx.doi.org/10.1016/j.icarus.2016.12.002

location). In the framework of our model, such differences would imply a different heat flux history released by the rock and metallic core as well as different interactions at the interface between this core and the HP ice mantle. While the dynamics of the HP ice does not directly affect the surface activity, the melt production and the associated chemical transfer through the HP mantle will control the thermo-compositional evolution of the ocean. The history of ocean crystallization then affects the internal dynamics of the outer ice shell and the associated surface activity. Geophysical measurements onboard the JUICE mission (Grasset et al., 2013) will provide essential constraints on the hydrosphere structure and composition, at present. Morphological and compositional mapping of Ganymede's surface will constrain its past history. The dynamical processes described in this study will help designing models of the thermo-chemical evolution of the moon leading to the present-day state.

Acknowledgements

We thank Hauke Hussmann and an anonymous reviewer for helpful reviews. The research leading to these results has received financial support from the European Research Council under the European Community's Seventh Framework Programme FP7/2007-2013, Grant Agreement no. 259285 (GC, GT,OG). GC, GT and OG also benefited from CNES funding to prepare the JUICE mission. This work was partly performed at the Jet Propulsion Laboratory (JPL), California Institute of Technology, under contract to NASA. CS acknowledges support by the NAI Icy worlds. KK acknowledges support by the office of the JPL Chief Scientist. Numerical simulations were performed on CCIPL facilities in Nantes (France).

References

Andersson, O., Inaba, A., 2014. Thermal conductivity of crystalline and amorphous ices and its implications on amorphization and glassy water. Phys. Chem. Chem. Phys. 7 (7), 1441–1449.
Baland, R.-M., Tobie, G., Lefèvre, A., Van Hoolst, T., 2014. Titan's internal structure inferred from its gravity field, shape, and rotation state. Icarus 237, 29–41.
Bargen, N., Waff, H.S., 1986. Permeabilities, interfacial areas and curvatures of partially molten systems: results of numerical computations of equilibrium microstructures. J. Geophys. Res. 91 (B9), 9261–9276.
Béghin, C., Randriamboarison, O., Hamelin, M., Karkoschka, E., Sotin, C., Whitten, R.C., Berthelier, J.-J., Grard, R., Simões, F., 2012. Analytic theory of titan's schumann resonance: constraints on ionospheric conductivity and buried water ocean. Icarus 218 (2), 1028–1042.
Bezacier, L., Journaux, B., Perrillat, J.P., Cardon, H., Hanfland, M., Daniel, I., 2014. Equations of state of ice VI and ice VII at high pressure and high temperature. J. Chem. Phys. 141 (10), 10405.
Bollengier, O., Choukroun, M., Grasset, O., Le Menn, E., Bellino, G., Morizet, Y., Tobie, G., 2013. Phase equilibria in the h 2 o-CO 2 system between 250-330k and 0–1.7 GPa: stability of the CO 2 hydrates and h 2 o-ice VI at CO 2 saturation. Geochim. Cosmochi. Acta 119, 322–339.
Bridgman, P., 1937. The phase diagram of water to 45,000 kg/cm2. J. Chem. Phys. 5 (12), 964–966.
Castillo-Rogez, J.C., Lunine, J.I., 2010. Evolution of titan's rocky core constrained by cassini observations. Geophys. Res. Lett. 37 (20).
Choblet, G., 2005. Modelling thermal convection with large viscosity gradients in one block of the cubed sphere. J. Comput. Phys. 205, 269–291.
Choblet, G., 2012. On the scaling of heat transfer for mixed heating convection in a spherical shell. Phys. Earth Planet. Inter. 206, 31–42.
Choblet, G., Parmentier, E., 2009. Thermal convection heated both volumetrically and from below: implications for predictions of planetary evolution. Phys. Earth Planet. Inter. 173, 290–296.
Choblet, G., Sotin, C., 2001. Early transient cooling of mars. Geophys. Res. Lett. 28, 3035–3038.
Choblet, G., Čadek, O., Couturier, F., Dumoulin, C., 2007. ŒDIPUS: a new tool to study the dynamics of planetary interiors. Geophys. J. Int. 170, 9–30.
Choukroun, M., Grasset, O., 2007. Thermodynamic model for water and high-pressure ices up to 2.2 gpa and down to the metastable domain. J. Chem. Phys. 127 (12), 124506.
Choukroun, M., Grasset, O., 2010. Thermodynamic data and modeling of the water and ammonia-water phase diagrams up to 2.2 gpa for planetary geophysics. J. Chem. Phys. 133 (14), 144502.
De La Chapelle, S., Milsch, H., Castelnau, O., Duval, P., 1999. Compressive creep of ice containing a liquid intergranular phase: rate-controlling processes in the dislocation creep regime. Geophys. Res. Lett. 26 (2), 251–254.
Deguen, R., 2012. Structure and dynamics of earth's inner core. Earth Planet. Sci. Lett. 333, 211–225.
Durham, W.B., Stern, L.A., Kirby, S.H., 1996. Rheology of water ices v and VI. J. Geophys. Res. 101 (B2), 2989–3001.
Golden, K.M., Ackley, S., Lytle, V., 1998. The percolation phase transition in sea ice. Science 282 (5397), 2238–2241.
Goldsby, D., Kohlstedt, D., 2001. Superplastic deformation of ice: experimental observations. J. Geophys. Res. 106, 11017–11030.
Grasset, O., Dougherty, M., Coustenis, A., Bunce, E., Erd, C., Titov, D., Blanc, M., Coates, A., Drossart, P., Fletcher, L., et al., 2013. Jupiter icy moons explorer (juice): an esa mission to orbit ganymede and to characterise the jupiter system. Plan. Space Sci. 78, 1–21.
Grasset, O., Schneider, J., Sotin, C., 2009. A study of the accuracy of mass-radius relationships for silicate-rich and ice-rich planets up to 100 earth masses. Astrophys. J. 693 (1), 722.
Grasset, O., Sotin, C., Deschamps, F., 2000. On the internal structure and dynamics of titan. Plan. Space Sci. 48 (7), 617–636.
Hudleston, P.J., 2015. Structures and fabrics in glacial ice: a review. J. Struct. Geol. 81, 1–27.
Hussmann, H., Sotin, C., Lunine, J.I., 2015. 10.18 interiors and evolution of icy satellites. In: Schubert, G. (Ed.), Treatise on Geophysics. Elsevier, Oxford, pp. 605–635. Second edition Edition
Iess, L., Jacobson, R.A., Ducci, M., Stevenson, D.J., Lunine, J.I., Armstrong, J.W., Asmar, S.W., Racioppa, P., Rappaport, N.J., Tortora, P., 2012. The tides of titan. Science 337 (6093), 457–459.
Journaux, B., Daniel, I., Caracas, R., Montagnac, G., Cardon, H., 2013. Influence of NaCL on ice VI and ice VII melting curves up to 6GPa, implications for large icy moons. Icarus 226 (1), 355–363.
Kalousová, K., Sotin, C., Tobie, G., Choblet, G., Grasset, O., 2015. Two-phase convection in the high-pressure ice layer of the large icy moons: geodynamical implications. AGU Fall meeting, P31C-2078
Kalousová, K., Souček, O., Tobie, G., Choblet, G., Čadek, O., 2014. Ice melting and downward transport of meltwater by two-phase flow in europa's ice shell. J. Geophys. Res. 119, 532–549.
Kamata, S., Matsuyama, I., Nimmo, F., 2015. Tidal resonance in icy satellites with subsurface oceans. J. Geophys. Res. 120 (9), 1528–1542.
Kargel, J.S., Kaye, J.Z., Head, J.W., Marion, G.M., Sassen, R., Crowley, J.K., Ballesteros, O.P., Grant, S.A., Hogenboom, D.L., 2000. Europa's crust and ocean: origin, composition, and the prospects for life. Icarus 148 (1), 226–265.
Khurana, K., Kivelson, M., Stevenson, D., Schubert, G., Russell, C., Walker, R., Polanskey, C., 1998. Induced magnetic fields as evidence for subsurface oceans in europa and callisto. Nature 395 (6704), 777–780.
Kirk, R., Stevenson, D., 1987. Thermal evolution of a differentiated ganymede and implications for surface features. Icarus 69 (1), 91–134.
Kivelson, M., Khurana, K., Volwerk, M., 2002. The permanent and inductive magnetic moments of ganymede. Icarus 157 (2), 507–522.
Lammer, H., Bredehöft, J., Coustenis, A., Khodachenko, M., Kaltenegger, L., Grasset, O., Prieur, D., Raulin, F., Ehrenfreund, P., Yamauchi, M., et al., 2009. What makes a planet habitable? Astron. Astrophys. Rev. 17 (2), 181–249.
Lefevre, A., Tobie, G., Choblet, G., Čadek, O., 2014. Structure and dynamics of Titan's outer icy shell constrained from Cassini data. Icarus 237, 16–28.
Lindkvist, J., Holmström, M., Khurana, K.K., Fatemi, S., Barabash, S., 2015. Callisto plasma interactions: hybrid modeling including induction by a subsurface ocean. J. Geophys. Res. 120 (6), 4877–4889.
McKinnon, W.B., 2006. On convection in ice i shells of outer solar system bodies, with detailed application to callisto. Icarus 183 (2), 435–450.
Mitri, G., Meriggiola, R., Hayes, A., Lefevre, A., Tobie, G., Genova, A., Lunine, J.I., Zebker, H., 2014. Shape, topography, gravity anomalies and tidal deformation of titan. Icarus 236, 169–177.
Monnereau, M., Dubuffet, F., 2002. Is Io's mantle really molten? Icarus 158, 450–459.
Moore, W.B., Webb, A.A.G., 2013. Heat-pipe Earth. Nature 501, 501–505.
Mueller, S., McKinnon, W.B., 1988. Three-layered models of ganymede and callisto: compositions, structures, and aspects of evolution. Icarus 76 (3), 437–464.
Niemann, H., Atreya, S., Demick, J., Gautier, D., Haberman, J., Harpold, D., Kasprzak, W., Lunine, J., Owen, T., Raulin, F., 2010. Composition of titan's lower atmosphere and simple surface volatiles as measured by the cassini-huygens probe gas chromatograph mass spectrometer experiment. J. Geophys. Res. 115 (E12).
Noack, L., Höning, D., Rivoldini, A., Heistracher, C., Zimov, N., Journaux, B., Lammer, H., Van Hoolst, T., Bredehöft, J., 2016. Water-rich planets: how habitable is a water layer deeper than on Earth? Icarus. in press
O'Reilly, T.C., Davies, G.F., 1981. Magma transport of heat on Io - a mechanism allowing a thick lithosphere. Geophys. Res. Lett. 8, 313–316.
Poirier, J., Sotin, C., Peyronneau, J., 1981. Viscosity of high-pressure ice vi and evolution and dynamics of ganymede. Nature.
Saur, J., Duling, S., Roth, L., Jia, X., Strobel, D.F., Feldman, P.D., Christensen, U.R., Retherford, K.D., McGrath, M.A., Musacchio, F., et al., 2015. The search for a subsurface ocean in ganymede with hubble space telescope observations of its auroral ovals. J. Geophys. Res. 120 (3), 1715–1737.
Schubert, G., Zhang, K.K., Kivelson, M.G., Anderson, J.D., et al., 1996. The magnetic–field and internal structure of ganymede. Nature 384 (6609), 544–545.
Showman, A.P., Stevenson, D.J., Malhotra, R., 1997. Coupled orbital and thermal evolution of ganymede. Icarus 129 (2), 367–383.
Sohl, F., Hussmann, H., Schwentker, B., Spohn, T., Lorenz, R., 2003. Interior structure models and tidal love numbers of titan. J. Geophys. Res. 108 (E12).

Sotin, C., Gillet, P., Poirier, J., 1985. Creep of high-pressure ice vi. In: Ices in the Solar System. Springer, pp. 109–118.
Sotin, C., Grasset, O., Mocquet, A., 2007. Mass–radius curve for extrasolar earth-like planets and ocean planets. Icarus 191 (1), 337–351.
Sotin, C., Tobie, G., 2004. Internal structure and dynamics of the large icy satellites. C. R. Physique 5 (7), 769–780.
Tchijov, V., 2004. Heat capacity of high-pressure ice polymorphs. J. Chem. Phys. 65, 851–854.
Tobie, G., Choblet, G., Sotin, C., 2003. Tidally heated convection: constraints on europa's ice shell thickness. J. Geophys. Res. 108, 5124.
Tobie, G., Grasset, O., Lunine, J.I., Mocquet, A., Sotin, C., 2005. Titan's internal structure inferred from a coupled thermal-orbital model. Icarus 175, 496–502.
Tobie, G., Lunine, J.I., Sotin, C., 2006. Episodic outgassing as the origin of atmospheric methane on Titan. Nature 440, 61–64.
Turcotte, D.L., 1989. A heat pipe mechanism for volcanism and tectonics on venus. J. Geophys. Res. 94 (B3), 2779–2785.
Vance, S., Bouffard, M., Choukroun, M., Sotin, C., 2014. Ganymede's internal structure including thermodynamics of magnesium sulfate oceans in contact with ice. Plan. Space Sci. 96, 62–70.
Vance, S., Harnmeijer, J., Kimura, J., Hussmann, H., DeMartin, B., Brown, J.M., 2007. Hydrothermal systems in small ocean planets. Astrobiology 7 (6), 987–1005.

Please cite this article as: G. Choblet et al., Heat transport in the high-pressure ice mantle of large icy moons, Icarus (2016), http://dx.doi.org/10.1016/j.icarus.2016.12.002